

Physical synchronization of soft self-oscillating limbs for fast and autonomous locomotion

Alberto Comoretto¹, Harmannus A.H. Schomaker,¹ Johannes T.B. Overvelde^{1,2*}

¹Autonomous Matter Department, AMOLF,
Science Park 104, 1098 XG Amsterdam, The Netherlands

²Institute for Complex Molecular Systems,
Department of Mechanical Engineering, Eindhoven University of Technology,
PO Box 513, 5600 MB Eindhoven, The Netherlands

*To whom correspondence should be addressed; E-mail: overvelde@amolf.nl.

Animals achieve robust locomotion by offloading regulation from the brain to physical couplings within the body. Contrarily, locomotion in artificial systems often depends on centralized processors. Here, we introduce a rapid and autonomous locomotion strategy with synchronized gaits emerging through physical interactions between self-oscillating limbs and the environment, without control signals. Each limb is a single soft tube that only requires constant flow of air to perform cyclic stepping motions at frequencies reaching 300 hertz. By combining several of these self-oscillating limbs, their physical synchronization enables tethered and untethered locomotion speeds that are orders of magnitude faster than comparable state-of-the-art. We demonstrate that these seemingly simple devices exhibit autonomy, including obstacle avoidance and phototaxis, opening up avenues for robust and functional robots at all scales.

Nature masters the complex problem of locomotion through embodied solutions, harnessing the synergy between the nervous system, body, and environment (1). The foundation of animal locomotion lies in the periodic and asymmetric motion of individual limbs (2, 3) (Fig. 1A). Multiple oscillating limbs are typically coordinated through a variety of embodied mechanisms, which are computationally and metabolically inexpensive as they diminish, or even eliminate, the need for sequential individual inputs from a central brain (3). For instance, stick insects achieve synchronized walking gaits through both explicit local neural connections and implicit body-environment interactions, avoiding centralized patterning (4) (Fig. 1B). Sea stars explicitly coordinate their five arms in a decentralized fashion through a nerve ring (5) (Fig. 1C). Moreover, sea stars occasionally exhibit a fast bouncing gait as an escape response, with their hundreds of tube feet achieving synchronization through implicit mechanical coupling with the external substrate (6) (Fig. 1C).

Inspired by nature, robots can delegate the locomotion task to their bodies (7), thus minimizing energy and time costs associated with a central computer. For instance, by harnessing the dynamics of the body, rigid robots based on passive-dynamic walkers reduce, but do not eliminate, the amount of control required for locomotion (8). Without processors, soft robots based on twisting liquid crystal elastomers (9) and elasto-active structures (10) leverage body-environment interactions to move forward and harness shape reconfiguration to avoid obstacles autonomously. However, due to the lack of limbs, their applicability is limited to specific tasks and environments (11), in contrast to the wide spectrum of robust behaviors typical of animals, which is often enabled by interactions between multiple self-oscillators (12).

Among soft-limbed robots, fluidic circuits (13) sequence walking gaits (14–17) without the need for electronic processors. However, fluidic circuits still emulate their electronic counterpart (18), involving multiple, macroscopic, digital or analog components that deliver sequential control signals in a quasi-static fashion. This architecture leads to energy losses and delay across the fluidic network, causing slow sequencing of the limbs in the order of one hertz, with consequent ineffective locomotion of only a few body lengths (BLs) per minute (14–17, 19–23), which is impractical for most real-world applications (24–26). Moreover, autonomous behavior of walkers with fluidic processors remains elusive, with the exception of one-time-use

touch sensing (15) and reprogrammable sequencing of non-integrated soft fingers (16).

In this work, inspired by the movement strategies of animals, we introduce a physical locomotion strategy that realizes rapid, self-coordinating gaits by harnessing implicit coupling through environmental interaction (Fig. 1D) and explicit coupling via embodied fluidic interconnections (Fig. 1E) of soft, self-oscillating limbs. With this approach, we can harness emerging synchronization between limbs to achieve orders of magnitude faster locomotion than existing comparable soft robots with internal control (17), and similar in speed to the fastest soft robots that use any external control technology (27) (Fig. 1F). Our mechanofluidic devices display autonomy, such as phototaxis (Fig. 1G), while not requiring either electronic or electronic-like mechanical (28) or fluidic (18) processors.

The self-oscillating limb To enable rapid locomotion without a central processor, here we develop a limb that undergoes full-step motion by harnessing a self-oscillating behavior of thin soft tubes, analogous to oscillations occurring in flat tubes with flowing water (29), and reminiscent of promotional air dancers (30) often seen by the roadside. We build the limb by simply bending a thin-walled commercial silicone tube 180° and constraining it at the inlet and outlet in a 3D-printed holder (Fig. 1H and fig. S1). If no airflow is provided, the tube displays two stable states with either one (31) or two kinks (Fig. 1H,I). Interestingly, when we apply a constant airflow $Q_{\text{in}} = 15$ SLPM to the inlet on the left side of the tube, the tube starts to spontaneously oscillate between the states with one and two kinks, at a frequency of approximately 100 Hz (Fig. 1J and movie S1).

Importantly, the motion of the tube during the oscillation cycle is intrinsically asymmetric. The tip of the limb, which we define as the point on the tube closest to a defined surface (Fig. 1K), traces a hysteretic trajectory in the x - y plane orthogonal to the surface (Fig. 1L). The tube, therefore, acts as a limb that undergoes a full-step motion, with a periodic closed-loop sequence of stance and swing phases (Fig. 1L and movie S1), reminiscent of animals' limbs (3) (Fig. 1A), where we have optimized the stance stroke by rotating the limb with respect to the surface (fig. S8). For constant input airflow, we delegate both the oscillation generation

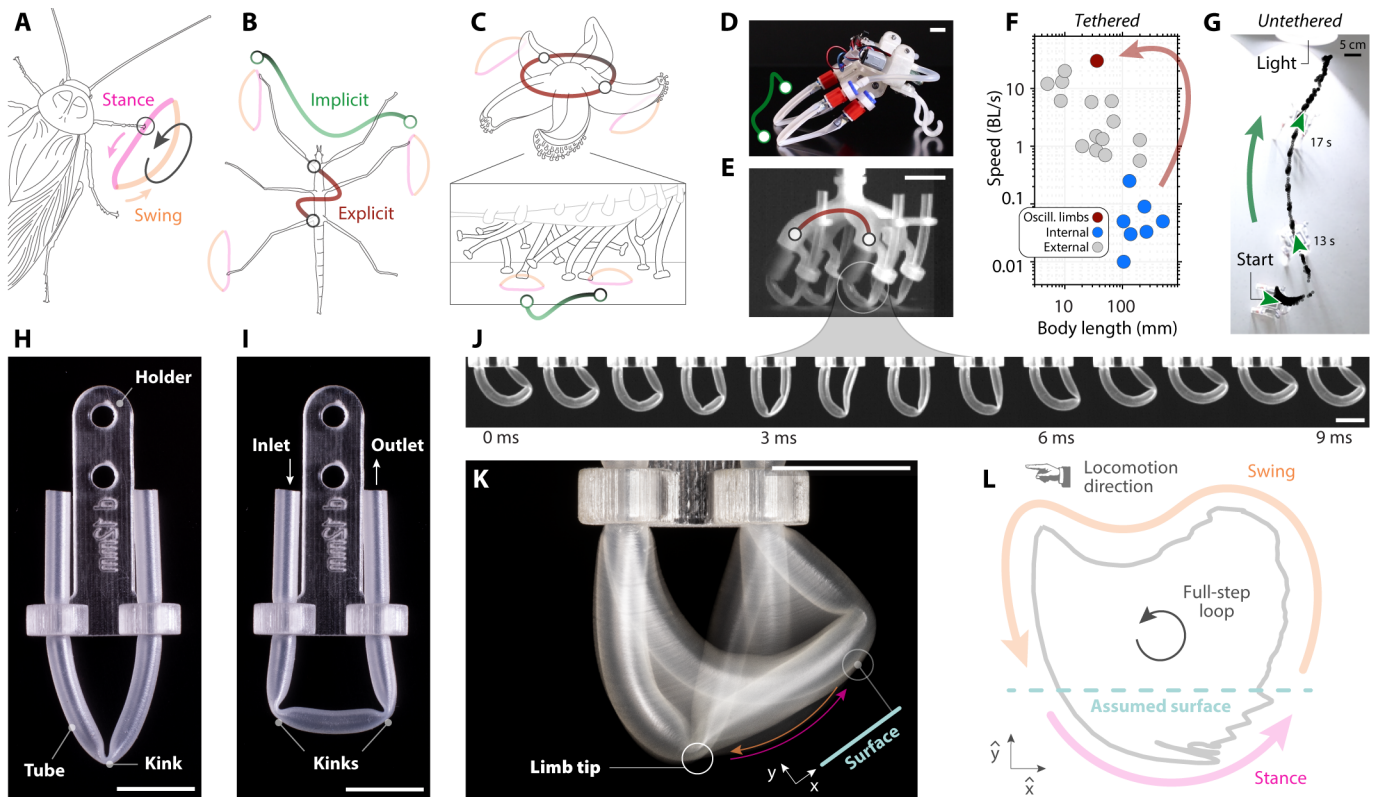


Figure 1: Like animals, our mechanofluidic robots move by physically coupling self-oscillating limbs that cyclically perform full-step motions. (A) Animals move through a periodic and asymmetric motion of their limbs (2, 3), with a sequence of stance and swing phases. Animals, e.g. (B) the stick insect and (C) the sea star, coordinate multiple oscillating limbs via explicit coupling through neural connections or implicit coupling through interaction with the environment (4–6). We exploit these forms of coupling between self-oscillating limbs in (D) untethered and (E) tethered mechanofluidic robots, that (F) move two orders of magnitude faster than comparable state-of-the-art robots with internal control (17), and (G) display autonomy capabilities, such as phototaxis. Our individual limb is a soft tube bent 180° that, in static conditions, displays (H) one or (I) two kinks. (J) When constant airflow $Q_{in} = 15$ SLPM is provided at the inlet on the left end, the tube self-oscillates at a frequency of 115 Hz (snapshots of one oscillation cycle). (K) The tip of the limb is the point on the tube closest to a defined surface (photograph with 0.5 s exposure time, capturing ~ 50 consecutive oscillations). (L) The tip cyclically undergoes a full-step loop trajectory, with a stance phase followed by a swing phase (the reported tip trajectory coordinates are normalized). Wherever not otherwise stated, scale bars are 1 cm.

and the sequencing of the tip motion within each cycle directly to the limb itself, surpassing the so-far-needed requirement of additional circuitry (13), either fluidic (15, 17) or electronic (32).

We next aim to empirically understand the behavior of the kink waves in the limb. To do so, we detect

the outer and inner edges of the tube (Fig. 2A and Supplementary Material section M3) and map the edges on a new coordinate system that follows the center line of the tube (Fig. 2B and fig. S10). Focusing on the local minima of the tube width, we can identify the existence of one or two kinks along the tube (Fig. 2B and movie S2). We refer to the kink with the smallest width as the dominant kink, and the second kink (if it exists at that moment in time) as the non-dominant kink.

From the location in time of the dominant and non-dominant kink (Fig. 2C and fig. S10), and the pressure at the inlet of the tube (Fig. 2D), we can identify four key steps during a single oscillation cycle. First, at ~ 5 ms (Fig. 2E) we observe two kinks that stay approximately at the same location on the tube until ~ 35 ms (Fig. 2F). During this time, the pressure at the inlet monotonically decreases, causing the non-dominant kink to increasingly sharpen (fig. S17). Second, between ~ 35 ms and ~ 40 ms the non-dominant kink becomes dominant, while the dominant kink becomes non-dominant and starts to disappear (fig. S10). At ~ 40 ms the non-dominant kink has completely disappeared (Fig. 2G). Third, we observe that the only kink in the tube starts to move away from the inlet, until ~ 60 ms (Fig. 2H). This traveling of the kink is the result of an increase of pressure at the inlet (fig. S12). Finally, after ~ 60 ms, a second kink starts to form upstream again due to an increase in bending moment (fig. S17). Note that this state (equivalent to figure 2E) is characterized by a lower fluidic resistance than the single kink state in Fig. 2G, since both kinks have a larger angle (fig. S17). This lower resistance causes pressure to drop again, such that the cycle repeats.

Therefore, we observe that for a continuous inflow of air, the internal pressure decreases and increases depending on the kink's state, since the change in cross-sectional area affects the local flow resistance of the tube (31). In turn, the pressure decrease favors kink growth, and the pressure increase causes kink travel. This interaction between tube inflation, kink formation and travel, and change in tube resistance sets up a hysteric actuation loop (fig. S12) that results in the self-oscillating behavior at constant inflow.

The frequency of the self-oscillation can be tuned by varying the flowrate through the tube. When we sweep the inflow between 0 and 20 SLPM, we observe three domains, with sharp transitions between them (Fig. 2I). For inflow values below ~ 3.8 SLPM, the tube leaks and does not oscillate (fig. S11), because

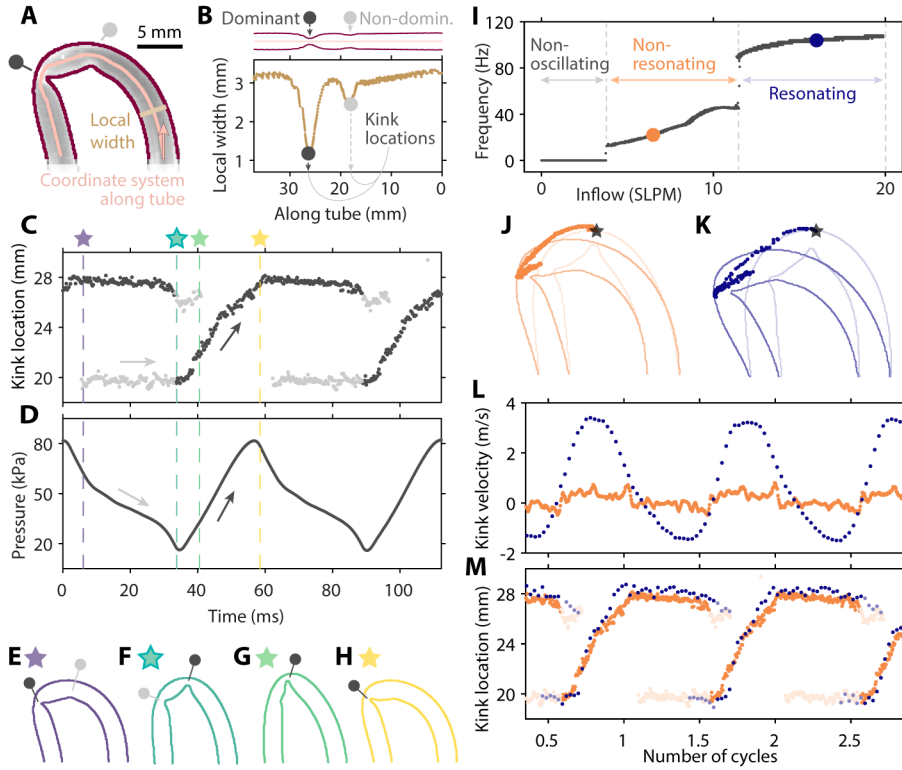


Figure 2: **Interplay between pressure and kinks' state enables self-oscillation, resonance enables high frequency.** (A) Detected edges of the tube (dark red) and coordinate system along the tube (pink). (B) The kinks correspond to the local minima (grey and black dots) of the local width along the tube. The (C) location of the kinks along the tube and (D) pressure inside the tube are coupled. (E, F, G, H) State of the tube at four instants of the oscillating cycle. (I) The oscillation frequency displays three regimes for different inflow rates. The tube has higher structural displacement in the (J) resonating domain than in the (K) non-resonating domain, as shown by the kink covering a larger distance. (L) In the resonating case, the structure undergoes high quasi-sinusoidal velocities, in comparison to the near-zero velocities of the non-resonating case. (M) The kink locations along the tube itself, for the two cases, overlap.

pressure cannot build up to make the kink travel (fig. S12). For flowrates between ~ 3.8 and ~ 11.4 SLPM, the system oscillates at frequencies between ~ 13 and ~ 45 Hz. Interestingly, for even higher flowrates the frequency suddenly jumps to higher frequencies above ~ 90 Hz.

This last sudden jump in frequency seems to be the result of structural resonance that starts to occur at flowrates above ~ 11.4 SLPM (movie S2). This can be seen from the increase in the distance traveled by the kink (Fig. 2J,K and fig. S10) and by the dramatic increase in the kink velocity, that approaches a sinusoidal

trend (Fig. 2L) (Supplementary Material section M3 for the definitions of kink distance and velocity). In comparison, the kink location along the tube does not undershoot or overshoot when the flow is increased (Fig. 2M), therefore not constituting the origin of the sudden increase in frequency. We conclude that, around the transition at ~ 11.4 SLPM, the resonance of the structure can be exploited to significantly increase the oscillation frequency, for a relatively small increase in input flowrate.

Explicit internal coupling of multiple limbs for ultrafast locomotion The individual self-oscillating limb shown so far becomes of practical robotic use only when integrated with other limbs in a multi-limbed system. With the goal of synchronizing the activation of several limbs to generate specific gaits, we couple two limbs by connecting them in parallel to a single input, using two identical coupling tubes (Fig. 3A). Surprisingly, when providing a constant airflow to the inlet we observe that shorter coupling tubes with an inner diameter of 2 mm lead to in-phase synchronization. The result is that the two kinks travel simultaneously (Fig. 3B) and the pressure signals align (Fig. 3C and movie S3), even though the natural frequencies of the two actuators are not identical and differ by ~ 5 Hz (fig. S13). In contrast, longer coupling tubes result in anti-phase synchronization where the actuators alternatively activate with a phase shift of $\sim 180^\circ$ (Fig. 3D,E and movie S3).

This synchronization effect is reminiscent of strong coupling between the two oscillators (33). In soft systems, strong coupling has previously been observed in mechanically-coupled liquid crystalline oscillators (34). Interestingly, here the coupling is induced by the fluidic interconnections. When scanning a wide range of the coupling tubes' length, we note a sharp transition between the in-phase and anti-phase eigenmodes (Fig. 3F,G). When the system is placed at this transition, we witness an alternating behavior where the two actuators continuously switch between the in-phase and anti-phase eigenmodes (violin plot at 12 cm in Fig. 3G, fig. S13 and movie S3).

Based on these findings, we build a robot with four strongly-coupled self-oscillating limbs, assembled onto a 3D-printed body with short inner channels with length ~ 1.5 cm, connected in parallel to a single tether (Fig. 3H, fig. S3 and fig. S4). Note that we orient the limbs with a 30° angle to the surface to optimize

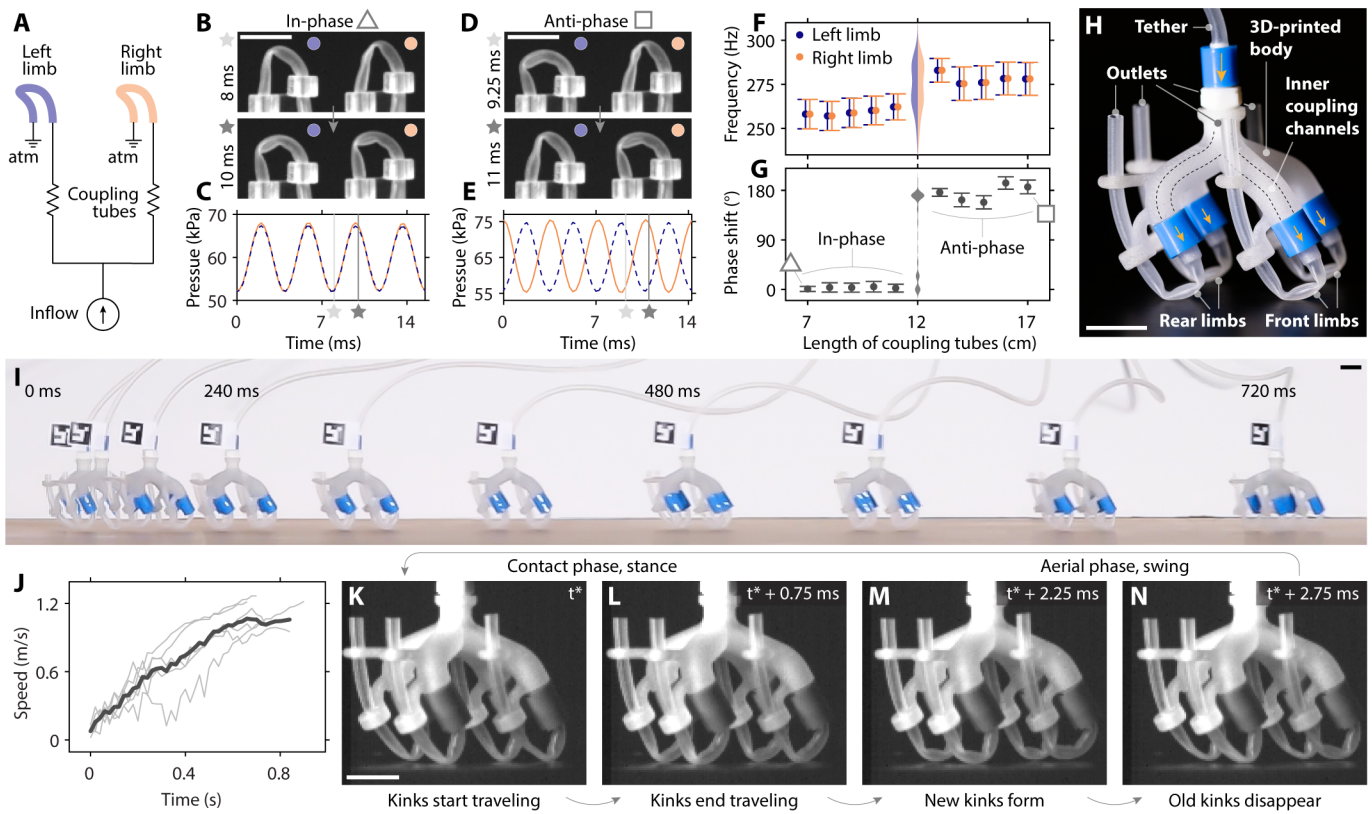


Figure 3: Synchronization of multiple limbs through explicit, internal coupling for ultrafast mechanofluidic robots. (A) We couple two limbs in parallel to the same input flow source of 15 SLPM with two identical silicone tubes. We observe in-phase synchronization, with (B) simultaneous kink traveling and (C) aligned pressure signals, or anti-phase synchronization, with (D, E) alternate activation of the limbs. We scan the length of the coupling tubes, observing two separated in-phase and anti-phase domains, as (F) the oscillation frequency of left and right limbs match, and (G) the phase-shift is either $\sim 0^\circ$ or $\sim 180^\circ$. (H) The tethered robot has four limbs connected to a 3D-printed monolithic body, with four inner coupling channels. (I) The robot achieves ultrafast locomotion on a flat surface. (J) Speed of the robot for six runs (grey) and mean speed (black). The four limbs, within ~ 3 ms, simultaneously go through a (K, L) stance phase, followed by a (M, N) swing phase. All scale bars are 1 cm.

the effective stance (fig. S8). When we provide a constant inflow of ~ 28 SLPM to the tether (fig. S6), the robot accelerates (Fig. 3I and movie S4), reaching a steady-state speed of 30 ± 2.5 BL/s (1.1 m s^{-1}), with a response time of 0.66 s (Fig. 3J and fig. S6). This speed is two orders of magnitude higher than comparable state-of-the-art tethered robots with internal actuation sequencing (17), and similar to current ultrafast tethered soft robots that need external control (27) (Fig. 1F, fig. S7 and table S1). Our mechanofluidic robot approaches

— in terms of size, weight, and absolute speed — the performance of the animal cockroach (fig. S7), one of the fastest invertebrates relative to its size (35).

Looking closely at the gait in Figure 3K-N and movie S4, as expected, we observe that all the limbs autonomously activate in synchrony, since we designed short inner coupling channels. The robot runs with a stotting gait, typical of gazelles (36). We observe some initial transient asynchronous behavior before the robot achieves steady-state stotting (Fig. 3J and movie S4). Note that the four limbs oscillate at a frequency of ~ 300 Hz (Fig. 3K-N), about three times higher than the case of the single limb that we analyzed in Figure 2. We achieved this higher frequency by reducing the distance that the kinks must travel along the tube, selecting tubes that are smaller in diameter by a factor ~ 0.8 and shorter in length by a factor ~ 0.5 (Supplementary Material section S1).

Implicit environmental coupling for fast and autonomous locomotion Even though our robot achieved ultrafast locomotion without external control, so far, we still required a tether to provide a power of ~ 85 W (Supplementary Material section S1). At the moment, it is not possible to generate this power from a lightweight on-board pressure source, making this robot not directly suited for untethered applications. Here, we find that the main limitation comes from the required ~ 3.8 SLPM before the individual limb starts to oscillate (Fig. 2I). We hypothesize that an increase in kink resistance (i.e., a reduction in kink area) and a reduction in bending stiffness can reduce the minimal flow needed to achieve self-oscillating behavior, and thus could reduce the power required for untethered operation.

Therefore, we update the design of our tubes by heat-sealing two thermoplastic polyurethane (TPU) sheets along two parallel lines. We mount this TPU component to a hinge joint to obtain a self-oscillating pouch limb (fig. S2). This updated limb has a much higher flow resistance upon kinking (fig. S17) and performs the full-step oscillation (Fig. 4A) with a minimum input airflow of only 0.1 SLPM (fig. S14). Note that compared to the silicone tube limb, we observe a lower oscillation frequency of maximum ~ 3.5 Hz (fig. S14). This is likely due to the higher geometric volume of air required for the kink to travel (~ 2.5 mL compared to

~ 0.04 mL, Supplementary Material section S2) which leads to a longer kink traveling time, and the absence of a resonant mode. However, this frequency reduction is compensated by a larger stroke per cycle of the pouch limb (Fig. 4B, fig. S14 and movie S1).

We next build an untethered robot with two pouch tubes as soft limbs, that are each independently powered with only ~ 0.2 W (Supplementary Material section S1) by a 3 V air pump, connected to a 3.7 V LiPo battery with 380 mA h (Fig. 4C, fig. S3 and fig. S4). The total weight of the assembled robot equals 76.7 g, which is ~ 6 times lower than the maximum force two pouch-based limbs can provide (fig. S15). When we turn the pumps on, we observe the robot autonomously, cyclically hopping at a rate of ~ 2 Hz, with each hopping cycle characterized by a stance phase (Fig. 4D,E) followed by a swing phase (Fig. 4F,G). The untethered robot covers ~ 6 body lengths in 3.2 s on a flat metal surface (movie S5), moving with a speed of 1.93 ± 0.07 BL/s (18.1 cm s^{-1}) (fig. S6), which is one order of magnitude faster than untethered soft fluidic robots (23), and comparable to the state-of-the-art untethered robots that implement any other soft technology (37) (fig. S7 and table S2).

Also in this untethered scenario, the robot's remarkably high speed is attributed to the synchronization of the soft limbs. However, in this case, synchronization emerges due to implicit interactions with the environment, and not through embedded fluidic connections as was the case for the tethered robot. In principle, we observe that the two limbs actuate at different natural frequencies and thus out of phase when placed upside down (Fig. 4H and movie S5). The different frequencies and phases result from manufacturing and other imperfections, as well as the fact that both limbs are independently powered with two distinct fluidic lines. When we flip the robot into the working position with the two limbs interacting with the ground, the limbs immediately start to actuate simultaneously and in-phase, while requiring higher pressures (Fig. 4I,J and movie S5). This in-phase synchronization is, therefore, due to the implicit coupling between the two oscillating soft limbs, induced by the rigid environment — which in this case is the ground — and the rigid, inertial body of the robot.

Harnessing such implicit environmental interactions to achieve synchronization enables autonomous be-

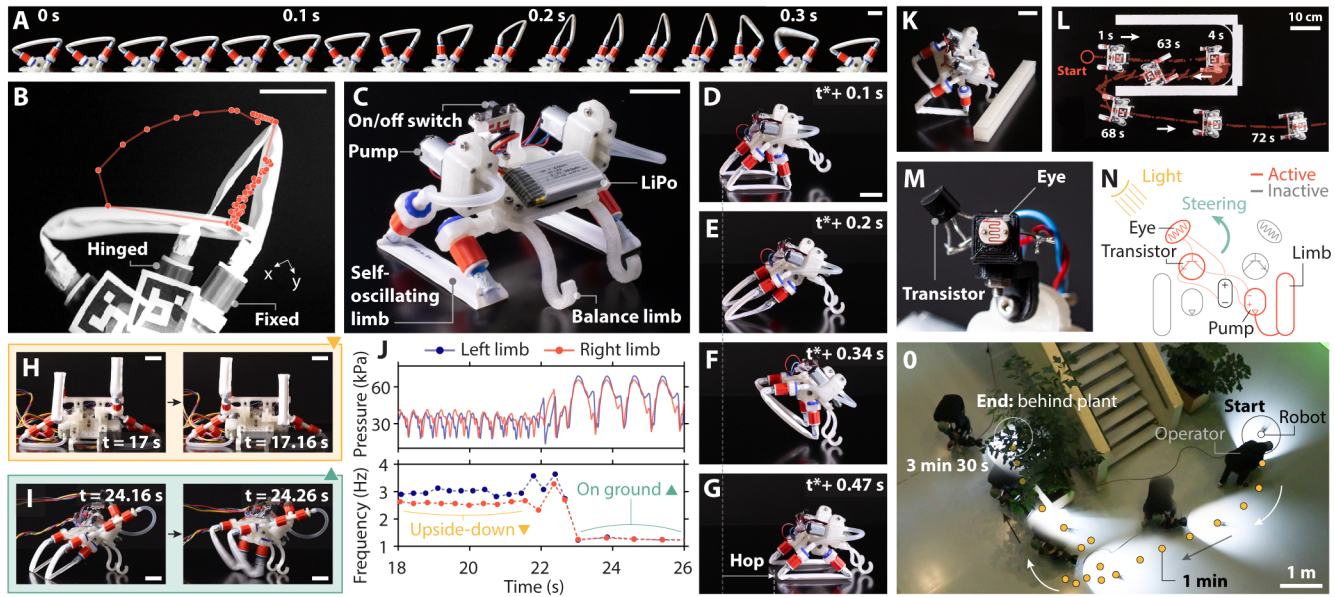


Figure 4: Synchronization of multiple limbs through implicit, environmental interaction for fast and autonomous mechanofluidic robots. The updated pouch limb (A) cyclically performs full-step motions with a low inflow of 0.3 SLPM, (B) displaying high hysteresis and stroke enabled by a hinge joint. (C) We mount two self-oscillating limbs on an untethered robot that carries a LiPo battery and a pump. The robot cyclically hops, with (D, E) a stance phase followed by (F, G) a swing phase. (H) The two limbs are not synchronized when the system is upside down. (I) When interacting with the ground, the two limbs synchronize. (J) While interacting, the pressure signals of the two limbs increase, and the frequencies equalize. (K) When encountering an obstacle, the mechanical cue temporarily affects the synchronization, resulting in the limbs activating asynchronously and the robot steering in place. (L) The robot harnesses consecutive mechanical cues to escape U-shaped obstructions autonomously. (M) We pair each pump with a transistor and a photoresistor as an eye. (N) Inspired by Braitenberg’s ‘aggressive vehicle’ (38), we cross-link the transistors and the pumps so that a limb is active when the opposite eye detects light. (O) This robot achieves autonomous phototaxis by steering in place when only one eye is active and hopping forward when both eyes are, following an operator that carries a light in a real-world environment. Wherever not otherwise stated, scale bars are 2 cm.

haviors, as interactions can affect the synchronization. For instance, when encountering an obstacle, the mechanical interaction between the body and an obstacle causes temporary asynchronous activation of the legs, resulting in the robot steering in place (Fig. 4K and movie S6). By harnessing these environmental cues, the robot can change behavior and autonomously escape a U-shaped obstruction, after noisy and consecutive random changes of direction (Fig. 4L and movie S6).

Still, since these body-obstacle interactions intrinsically lead to random outcomes as our system has not been specifically designed for effectively harnessing these interactions robustly (movie S6), we propose additional sensing that directly affects the self-oscillating behavior as a means to design predictable interactions and to achieve more reliable autonomy. To do so, we take inspiration from Braitenberg’s ‘aggressive vehicle 2b’ (38), and design internal neural interactions by equipping the robot with two ‘eyes’ (LDR light sensors) (Fig. 4M), each paired with a transistor that activates the opposite soft limb when the eye senses light (Fig. 4N). This relatively simple robot achieves autonomous phototaxis, as the synchronization behavior is affected such that it steers in place when only one eye detects light and implicitly coordinates the limbs to hop forward when both eyes do (Fig. 1G, fig S6 and movie S6). Outside of the lab, this allows the robot to move to a bright room from a darker one (movie S6) and to continuously follow an operator who carries a light (Fig. 4O and movie S6).

Concluding remarks In conclusion, we leverage kink waves in a soft tube to create a self-oscillating limb that cyclically performs a full-step motion at high frequencies. Inspired by nature, we blur the boundaries between actuation, control, and body-environment interaction by physically synchronizing multiple limbs through explicit internal coupling or implicit interaction with the environment, realizing rapidly-moving, autonomous mechanofluidic robots.

When implemented in other robotic domains, our decentralized locomotion strategy will open doors to useful and robust behaviors. The intrinsically asymmetric motion, combined with additional studies on synchronization across various environments, can open new avenues for amphibious locomotion (39) of under-actuated and under-controlled adaptive robots. The sub-watt power requirement holds strong potential for sustainable energy-harvesting robots (40). Further optimization of the individual limb morphology and the inter-limb interactions could result in high-performing actuator-controller integrated subsystems towards robots that outrun animals (41). Arrays of scaled-down self-oscillating limbs as active microscopic cilia (42) could set the foundation for microrobots in which autonomous behavior emerges from mechanical and fluidic inter-

actions alone, without relying on microelectronics (43). To this end, further exploration of the large design space of the internal and environmental interactions will result in vast behavioral complexity, since nonlinear systems are greatly affected by relatively small design changes (44). Going beyond control signals, physical synchronization lays the basis for robust and functional movement at all scales, with self-oscillating limbs as the basic building block to enable autonomous locomotion.

References

1. H. J. Chiel, R. D. Beer, The brain has a body: adaptive behavior emerges from interactions of nervous system, body and environment, *Trends in Neurosciences* **20**, 553-557 (1997).
2. A. J. Ijspeert, Biorobotics: Using robots to emulate and investigate agile locomotion, *Science* **346**, 196-203 (2014).
3. M. H. Dickinson, C. T. Farley, R. J. Full, M. A. R. Koehl, R. Kram, S. Lehman, How animals move: An integrative view, *Science* **288**, 100-106 (2000).
4. H. Cruse, V. Dürri, J. Schmitz, Insect walking is based on a decentralized architecture revealing a simple and robust controller, *Philosophical Transactions of the Royal Society A: Mathematical, Physical and Engineering Sciences* **365**, 221-250 (2007).
5. E. G. Clark, D. Kanauchi, T. Kano, H. Aonuma, D. E. G. Briggs, A. Ishiguro, The function of the ophiuroid nerve ring: how a decentralized nervous system controls coordinated locomotion, *Journal of Experimental Biology* **222**, jeb192104 (2019).
6. S. Heydari, A. Johnson, O. Ellers, M. J. McHenry, E. Kansa, Sea star inspired crawling and bouncing, *Journal of The Royal Society Interface* **17**, 20190700 (2020).
7. R. Pfeifer, M. Lungarella, F. Iida, Self-organization, embodiment, and biologically inspired robotics, *Science* **318**, 1088-1093 (2007).

8. S. Collins, A. Ruina, R. Tedrake, M. Wisse, Efficient bipedal robots based on passive-dynamic walkers, *Science* **307**, 1082-1085 (2005).
9. Y. Zhao, Y. Chi, Y. Hong, Y. Li, S. Yang, J. Yin, Twisting for soft intelligent autonomous robot in unstructured environments, *Proceedings of the National Academy of Sciences* **119**, e2200265119 (2022).
10. Y. Xi, T. J. Jones, R. Huang, T. Marzin, P. T. Brun, Emergent intelligence of buckling-driven elasto-active structures (2024).
11. M. H. Raibert, *Legged robots that balance* (MIT press, 1986).
12. A. J. Ijspeert, A. Crespi, D. Ryczko, J.-M. Cabelguen, From swimming to walking with a salamander robot driven by a spinal cord model, *Science* **315**, 1416-1420 (2007).
13. K. McDonald, T. Ranzani, Hardware methods for onboard control of fluidically actuated soft robots, *Frontiers in Robotics and AI* **8** (2021).
14. B. Gorissen, E. Milana, A. Baeyens, E. Broeders, J. Christiaens, K. Collin, D. Reynaerts, M. De Volder, Hardware sequencing of inflatable nonlinear actuators for autonomous soft robots, *Advanced Materials* **31**, 1804598 (2019).
15. D. Drotman, S. Jadhav, D. Sharp, C. Chan, M. T. Tolley, Electronics-free pneumatic circuits for controlling soft-legged robots, *Science Robotics* **6**, eaay2627 (2021).
16. L. C. van Laake, J. de Vries, S. Malek Kani, J. T. B. Overvelde, A fluidic relaxation oscillator for reprogrammable sequential actuation in soft robots, *Matter* **5**, 2898-2917 (2022).
17. S. Conrad, J. Teichmann, P. Auth, N. Knorr, K. Ulrich, D. Bellin, T. Speck, F. J. Tauber, 3d-printed digital pneumatic logic for the control of soft robotic actuators, *Science Robotics* **9**, eadh4060 (2024).

18. D. J. Preston, P. Rothemund, H. J. Jiang, M. P. Nemitz, J. Rawson, Z. Suo, G. M. Whitesides, Digital logic for soft devices, *Proceedings of the National Academy of Sciences* **116**, 7750-7759 (2019).
19. N. Vasios, A. J. Gross, S. Soifer, J. T. B. Overvelde, K. Bertoldi, Harnessing viscous flow to simplify the actuation of fluidic soft robots, *Soft Robotics* **7**, 1-9 (2020). PMID: 31070518.
20. H. Nabae, E. Kitamura, Self-excited valve using a flat ring tube: Application to robotics, *Frontiers in Robotics and AI* **9** (2022).
21. P. Rothemund, A. Ainla, L. Belding, D. J. Preston, S. Kurihara, Z. Suo, G. M. Whitesides, A soft, bistable valve for autonomous control of soft actuators, *Science Robotics* **3**, eaar7986 (2018).
22. W.-K. Lee, D. J. Preston, M. P. Nemitz, A. Nagarkar, A. K. MacKeith, B. Gorissen, N. Vasios, V. Sanchez, K. Bertoldi, L. Mahadevan, G. M. Whitesides, A buckling-sheet ring oscillator for electronics-free, multimodal locomotion, *Science Robotics* **7**, eabg5812 (2022).
23. C. J. Decker, H. J. Jiang, M. P. Nemitz, S. E. Root, A. Rajappan, J. T. Alvarez, J. Tracz, L. Wille, D. J. Preston, G. M. Whitesides, Programmable soft valves for digital and analog control, *Proceedings of the National Academy of Sciences* **119**, e2205922119 (2022).
24. O. D. Yirmibeşoğlu, T. Oshiro, G. Olson, C. Palmer, Y. Mengüç, Evaluation of 3d printed soft robots in radiation environments and comparison with molded counterparts, *Frontiers in Robotics and AI* **6** (2019).
25. M. Dunbabin, L. Marques, Robots for environmental monitoring: Significant advancements and applications, *IEEE Robotics & Automation Magazine* **19**, 24-39 (2012).
26. Y. Lu, X. Zhai, S. Saha, S. Ehsan, K. McDonald-Maier, A self-scrubbing scheme for embedded systems in radiation environments, *2020 IEEE 26th International Symposium on On-Line Testing and Robust System Design (IOLTS)* (2020), pp. 1–4.

27. Y. Wu, J. K. Yim, J. Liang, Z. Shao, M. Qi, J. Zhong, Z. Luo, X. Yan, M. Zhang, X. Wang, R. S. Fearing, R. J. Full, L. Lin, Insect-scale fast moving and ultrarobust soft robot, *Science Robotics* **4**, eaax1594 (2019).
28. H. Yasuda, P. R. Buskohl, A. Gillman, T. D. Murphey, S. Stepney, R. A. Vaia, J. R. Raney, Mechanical computing, *Nature* **598**, 39–48 (2021).
29. H. Tsukagoshi, A. Kitagawa, K. Tambo, H. Chiba, A fluid self-excited oscillation peculiar to flat ring tube and its application to wearable robots, *Proceedings 2007 IEEE International Conference on Robotics and Automation* (2007), pp. 3138–3139.
30. S. Dean, Biography of an inflatable tube guy, *Medium* (2014).
31. K. Luo, P. Rothemund, G. M. Whitesides, Z. Suo, Soft kink valves, *Journal of the Mechanics and Physics of Solids* **131**, 230-239 (2019).
32. M. T. Tolley, R. F. Shepherd, B. Mosadegh, K. C. Galloway, M. Wehner, M. Karpelson, R. J. Wood, G. M. Whitesides, A resilient, untethered soft robot, *Soft Robotics* **1**, 213-223 (2014).
33. A. Pikovsky, M. Rosenblum, J. Kurths, *Synchronization: A Universal Concept in Nonlinear Sciences*, Cambridge Nonlinear Science Series (Cambridge University Press, 2001).
34. G. Vantomme, L. C. M. Elands, A. H. Gelebart, E. W. Meijer, A. Y. Pogromsky, H. Nijmeijer, D. J. Broer, Coupled liquid crystalline oscillators in Huygens' synchrony, *Nature Materials* **20**, 1702-1706 (2021).
35. R. J. Full, M. S. Tu, Mechanics of A Rapid Running Insect: Two-, Four-and Six-Legged Locomotion, *Journal of Experimental Biology* **156**, 215-231 (1991).
36. F. R. Walther, Flight behaviour and avoidance of predators in Thomson's gazelle (*Gazella thomsoni* Guenther 1884), *Behaviour* **34**, 184–221 (1969).

37. Z. Xiong, Y. Su, H. Lipson, Fast untethered soft robotic crawler with elastic instability, *2023 IEEE International Conference on Robotics and Automation (ICRA)* (2023), pp. 2606–2612.
38. V. Braitenberg, *Vehicles: Experiments in Synthetic Psychology* (The MIT Press, 1986).
39. R. Baines, S. K. Patiballa, J. Booth, L. Ramirez, T. Sipple, A. Garcia, F. Fish, R. Kramer-Bottiglio, Multi-environment robotic transitions through adaptive morphogenesis, *Nature* **610**, 283-289 (2022).
40. F. Hartmann, M. Baumgartner, M. Kaltenbrunner, Becoming sustainable, the new frontier in soft robotics, *Advanced Materials* **33**, 2004413 (2021).
41. S. A. Burden, T. Libby, K. Jayaram, S. Sponberg, J. M. Donelan, Why animals can outrun robots, *Science Robotics* **9**, eadi9754 (2024).
42. M. S. Bull, L. A. Kroo, M. Prakash, Excitable mechanics embodied in a walking cilium (2021).
43. M. Z. Miskin, A. J. Cortese, K. Dorsey, E. P. Esposito, M. F. Reynolds, Q. Liu, M. Cao, D. A. Muller, P. L. McEuen, I. Cohen, Electronically integrated, mass-manufactured, microscopic robots, *Nature* **584**, 557-561 (2020).
44. L. C. van Laake, A. Comoretto, J. T. B. Overvelde, On the coexistence of pressure regulation and oscillation modes in soft hysteretic valves, *Journal of Fluids and Structures* **126**, 104090 (2024).

Acknowledgments

We thank all members of our Soft Robotic Matter Group for the invaluable discussions. We thank Corentin Coulais and Said RK Rodríguez for the constructive feedback. **Funding:** A.C., H.A.H.S., and J.T.B.O. acknowledge the European Union’s 2020 ERC-STG under grant agreement No. 948132. This work is part of the Dutch Research Council (NWO) and was performed at the research institute AMOLF. **Authors contributions:** A.C. and J.T.B.O. proposed and developed the research idea; A.C. designed and fabricated the devices;

A.C. and H.A.H.S. performed the experiments; A.C. and H.A.H.S. performed the data analysis; A.C. and J.T.B.O. wrote the manuscript; A.C., H.A.H.S., and J.T.B.O. revised the manuscript; J.T.B.O. supervised the research. **Competing interests:** A.C., H.A.H.S., and J.T.B.O. declare no competing interests.